BUTTERWORTH HEINEMANN

Polymer Vol. 36 No. 3, pp. 575–586, 1995

0032-3861/95/$10.00+0.00

A model for interdiffusion at interfaces of polymers with dissimilar physical properties

Esmaiel Jabbari and Nikolaos A. Peppas*
School of Chemical Engineering, Purdue University, West Lafayette, IN 47907, USA
(Received 29 March 1993; revised 2 August 1994)

A model was developed for interdiffusion at interfaces of polymers with dissimilar physical properties. This model is based on the assumption that the monomeric friction coefficients of the two polymers are identical but a strong function of the matrix composition. The composition dependence of the monomeric friction coefficient was evaluated from the blend zero-shear viscosity using the reptation theory. In turn, the compositional dependence of the blend zero-shear viscosity was evaluated using the volumetric properties of the blend and the free-volume theory. For polymers with dissimilar properties, this model predicts that the concentration profiles are highly asymmetric, with substantial swelling of the slower-diffusing component by the faster-diffusing component. This model also predicts the effect of changes in the volume of mixing on interdiffusion at polymer/polymer interfaces. The model was applied to a polymer pair with very dissimilar physical properties consisting of polystyrene and poly(vinyl methyl ether) and to a polymer pair with relatively similar properties consisting of poly(vinyl chloride) and poly(methyl methacrylate), to predict the concentration profile.

(Keywords: modelling; interdiffusion; polymer/polymer interface)

INTRODUCTION

Polymer/polymer interdiffusion affects the mechanical properties of polymers near interfaces. Applications include encapsulation of microelectronic devices, rubber-toughened polymer composites and welding of polymer interfaces[1,2]. In these applications the final properties of the polymer are determined by the thickness of the interface or the concentration profile of the two polymers across the interface. Interdiffusion at polymer/polymer interfaces is a strong function of temperature, composition, compatibility, molecular weight, molecular-weight distribution, chain orientation and molecular structure of the polymers[3–7]. In particular, differences in physical properties of the two polymers have a marked effect on the shape of the concentration profile as interdiffusion proceeds. For example, Brochard-Wyart and de Gennes[8,9] showed that in asymmetric conditions polymers reptate in a set of moving tubes. Brochard-Wyart and Pincus[10] showed that the initial asymmetry in the kinetics induced by the end segregation is healed after a characteristic Rouse time. In a previous paper[11], we showed experimentally that for polymer pairs with dissimilar physical properties the concentration profile can be highly asymmetric.

To describe the effect of the above parameters on interdiffusion, de Gennes[12] used the chemical potential gradient as the driving force for interdiffusion. Assuming the fluxes of the two components were equal but opposite, Brochard-Wyart *et al.*[13] derived the slow-mode theory for interdiffusion at polymer interfaces:

$$D=\left(\frac{\Lambda_A\Lambda_B}{\Lambda_A+\Lambda_B}\right)\left(\frac{1}{N_A\phi_A}+\frac{1}{N_B\phi_B}+2\chi\right) \quad (1)$$

*To whom correspondence should be addressed

Here, D is the interdiffusion coefficient, Λ_A and Λ_B are the mobilities of polymers A and B, respectively, N_A and N_B are the number of repeat units of each polymer, ϕ_A and ϕ_B are the molar fraction of each polymer, and χ is the Flory–Huggins interaction parameter. The slow-mode theory predicts that interdiffusion is dominated by the slower-diffusion polymer. Later, de Gennes[14] showed that the mobility was directly related to the tracer diffusion coefficient of each polymer. The limitation of this theory is that it assumes that the fluxes of the two polymers are equal and opposite, which means that the interface remains symmetric as interdiffusion proceeds for symmetric boundary conditions.

On the other side, Kramer and associates[15,16] showed that, for polymer pairs with different molecular weights, the interface moves towards the polymer with the lower molecular weight as interdiffusion proceeds. Kramer *et al.*[17] and Sillescu[18] described interdiffusion in systems with a moving interface by unequal fluxes of polymers A and B, which were balanced by a net flux of vacancies across the interface. By assuming that the chemical potential of vacancies was zero in the melt state but the flux of vacancies was finite, they derived the following equation for the interdiffusion coefficient:

$$D=\phi_A\phi_B\left(\frac{\phi_B}{\phi_A}\Lambda_A+\frac{\phi_A}{\phi_B}\Lambda_B\right)\left(\frac{1}{\phi_A N_A}+\frac{1}{\phi_B N_B}+2\chi\right) \quad (2)$$

In the fast-mode theory, the overall mobility is linearly related to the mobility of each component, indicating that the interdiffusion coefficient is dominated by the faster-moving component.

Akcasu *et al.*[19] attempted to identify the fast and slow modes with the two modes observed in dynamic scattering experiments from ternary polymer solutions.

They defined the vacancies as the third component in a mixture of A and B polymers and concluded that the slow mode was obtained when vacancies were gradually removed, resulting in an incompressible binary mixture of A and B. The fast mode was obtained in the opposite limit of high vacancy concentration or a matrix with very high mobility. Since the polymer mobility and the vacancy concentration are small below and high above T_g, this suggested that the slow- and fast-mode theories described interdiffusion below and above T_g, respectively.

In fact, most of the interdiffusion data in the literature[14-17,20,21] which were collected above the T_g of polymers, are consistent with the fast-mode theory of interdiffusion. Kramer *et al.*[17] used Rutherford back-scattering spectroscopy to follow the movement of a gold marker at the interface between polystyrene (PS) and deuterated polystyrene (d-PS) with different molecular weights. They observed movement of the interface towards the faster-diffusion component. Reiter *et al.*[22] used X-ray reflection spectrometry to follow the movement of a gold marker placed at the interface between PS/d-PS. They were able to detect a delay in the onset of interface movement, which depended on molecular weight, and there was a strong indication of a correlation between this induction time and the reptation time of the chain. Moreover, the marker velocity at times shorter than the reptation time of the long molecules was not influenced by the long molecules.

Using a statistical-mechanical approach, Foley and Cohen[23] showed that the mutual friction coefficient for the slow mode was the arithmetic mean of the friction coefficient of each component. On the other hand, the mutual friction coefficient for the fast mode was the geometric mean of the two components. This indicates that the slow- and fast-mode theories are applicable to homopolymers with different molecular weights or to polymers with similar physical properties.

Recent results from Sauer and Walsh[24] and our laboratory[11] have shown that, for polymer interfaces with dissimilar properties, the faster-diffusing component swells the slower-diffusing component at temperatures near the T_g of the slower-diffusing polymer. These results were obtained using a polymer pair consisting of polystyrene (PS) as the slower-diffusing component with T_g of 101°C and poly(vinyl methyl ether) (PVME) as the faster-diffusing component with T_g of −27°C. The concentration profile was highly asymmetric, which could not be described by the slow- or fast-mode theories.

The major drawback in using the fast- or slow-mode theories to predict the concentration profile at polymer/polymer interfaces is in relating the mobility of the polymers, Λ_A and Λ_B, to the properties of the matrix. For interdiffusion at homopolymer interfaces or interfaces between polymers with similar physical properties, the mobilities are relatively independent of composition across the interface. However, for polymers with dissimilar physical properties, the composition dependence of the mobilities has a significant effect on the concentration profile. For compatible polymers, since the matrix is homogeneous on a microscopic scale, there exists a relationship between the polymer mobilities that relates these mobilities to the properties of the matrix.

Here we present a model for interdiffusion at polymer/polymer interfaces for polymers with very dissimilar properties. This model is based on irreversible thermodynamics and accounts for the composition dependence of the tracer diffusion coefficients assuming the monomeric friction coefficients of the two polymers are identical but a strong function of composition. The composition dependence of the monomeric friction coefficients is evaluated from the volumetric properties of the blend, free-volume theory and the reptation theory.

THEORY

Description of the lattice

The interdiffusion pair is schematically shown in *Figure 1*. One phase consists of the polymer with low mobility (designated by s for 'slow') with vacancies randomly distributed in the lattice. The other phase consists of the polymer with high mobility (designated by f for 'fast'). It is assumed that the concentration of vacancies is a small fraction of the total concentration and does not contribute to the free energy of mixing. Since the polymers on each side of the interface have different molecular weights and chemical structures, there is a chemical potential gradient across the interface. The system is modelled by using this chemical potential gradient as the driving force for interdiffusion and assuming that the flux is one-dimensional in the direction perpendicular to the interface. We also invoke the assumption of quasi-equilibrium on a microscopic scale, which means that the polymer molecule is at equilibrium locally while interdiffusion takes place. This is a valid assumption for compatible polymers with diffusion lengths of the order of micrometres, which are at least two orders of magnitude greater than the radius of gyration of the polymer molecule.

Irreversible thermodynamic formulation

We adopt the Onsager formulation[25,26], which relates the flux of the species across the interface to the chemical potential gradient of each component:

$$j_i = \frac{-1}{RT}\sum_k \Lambda_{ik}\Delta\mu_k \qquad i,k = \text{s,f,v} \tag{3}$$

Here, subscripts, s, f and v stand for slow component, fast component and vacancies, respectively. The symbol j_i, a scalar, is the molar monomeric flux of component i for one-dimensional diffusion, T is the absolute temperature, R is the gas constant, μ_k is the molar

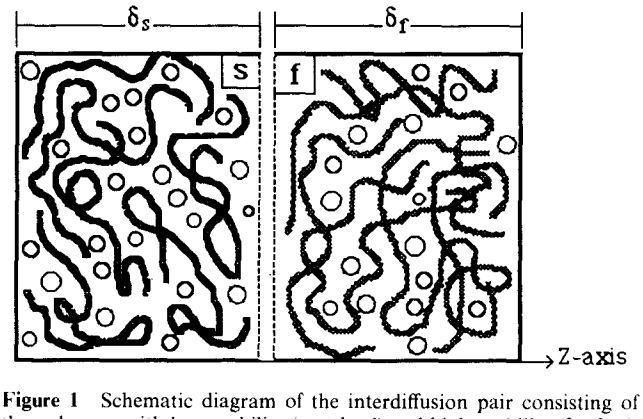

Figure 1 Schematic diagram of the interdiffusion pair consisting of the polymers with low mobility (s = 'slow') and high mobility (f = 'fast') with vacancies (○) distributed randomly in the lattice

monomeric chemical potential of component k, Λ_{ii} is the Onsager coefficient of component i, and Λ_{ik} is the cross-coefficient of component i due to the gradient of component k. In the above equations, the Onsager reciprocity[26,27] relations (e.g. $\Lambda_{ik}=\Lambda_{ki}$) are used to reduce the number of Onsager coefficients from nine to six.

From one-dimensional diffusion in the Cartesian coordinate system with negligible excess volume of mixing and no change in the lattice size, the sum of the three fluxes must be equal to zero. This relationship can be used to express the vacancy Onsager coefficients in terms of the coefficients of the other two components:

$$\Lambda_{iv}=-\sum_j \Lambda_{ij} \qquad i=\text{s,f,v};\ j=\text{s,f} \tag{4}$$

The cross-coefficients or the Onsager coefficient of component i due to the gradient of component k are only important in systems with electrostatic interactions and they can be evaluated by the condition of electroneutrality[28]. For interdiffusion in polymer pairs without ionic groups, such as poly(vinyl chloride)/poly(methyl methacrylate) (PVC/PMMA) or PS/PVME, the cross-coefficients can be neglected. Substituting for vacancy Onsager coefficients from equation (4) and neglecting the cross-coefficients results in the following relation between the fluxes and the chemical potential gradients:

$$j_i=\frac{\Lambda_{ii}}{RT}(\Delta\mu_i-\Delta\mu_v) \qquad i=\text{s,f} \tag{5}$$

The chemical potential of the vacancies is a measure of the mobility of a vacancy within the polymer matrix as compared with the surroundings[29]. This is related to the average relaxation time of a polymer chain as compared with the experimental time. If the chain relaxation time is of the same order of magnitude as the experimental time, then the chemical potential of vacancies is significant. On the other hand, if the chain relaxation time is fast compared with the experimental time, then the chemical potential of vacancies is negligible.

Experimental results from our laboratory[30] with the PS/PVME pair above the T_g of PS indicate that the diffusion process is independent of the molecular weight of the slower-diffusing component, PS, in support of the assumption that the chemical potential of vacancies is negligible. However, our experimental results below the T_g of PS indicate that the vacancy chemical potential may be significant below the T_g of the slower-diffusing component owing to stresses in the glassy state. Assuming that the chemical potential of vacancies is negligible compared with the chemical potential gradient across the interface, equation (5) reduces to the following:

$$j_i=\frac{\Lambda_{ii}}{RT}\Delta\mu_i \qquad i=\text{s,f} \tag{6}$$

Chemical potential gradient

The Flory–Huggins equation[31] is used to relate the chemical potential to the entropy and enthalpy of mixing of the two polymers. The polymer–vacancy interaction parameter is negligible. This is a good assumption since the concentration of vacancies is an order of magnitude lower than the polymer concentration. The molar monomeric chemical potential for each component is obtained from the derivative of total free energy with respect to the number of moles of that component, whereas the chemical potential gradient is obtained from the derivative of monomeric chemical potential with respect to the diffusion axis:

$$\Delta\mu_i=\frac{RT}{\phi_i}\left(\frac{1-\phi_s}{N_s}+\frac{\phi_s}{N_f}+2\chi_{sf}\phi_s(1-\phi_s)\right)\Delta\phi_i \qquad i=\text{s,f} \tag{7}$$

Here, χ_{sf} is the interaction parameter between a monomer of the slower- and faster-moving components, and N_s and N_f are the number of repeat units for the slower- and faster-moving components, respctively. Equation (7) relates the monomeric chemical potential gradient of each component to temperature, molecular weight of each polymer, compatibility parameter and composition.

Since the polymers are incompressible, the net exchange of matter across the interface as a result of different diffusion coefficients of the two polymers causes swelling of the slower-diffusing component by the fast-moving component. This swelling results in the movement of the interface as interdiffusion progresses. The amount of swelling is related to the net flux of vacancies across the interface. Therefore, the total flux of each component is given by the following relations:

$$j_i^t=j_i+\phi_i j_v \qquad i=\text{s,f} \tag{8}$$

Here, j_s^t and j_f^t, scalar quantities, are the total molar monomeric flux of the slower- and faster-diffusing components, respectively. A molar balance for each component results in the following equation relating the rate of change of flux as a function of distance to the rate of change of concentration as a function of time:

$$\frac{\partial\phi_i}{\partial t}=-\upsilon\frac{\partial j_i^t}{\partial z} \qquad i=\text{s,f} \tag{9}$$

where υ is the mobility.

Estimation of the Onsager coefficients

De Gennes[14] has shown that the Onsager coefficients for interdiffusion of polymer i due to a gradient of its own chemical potential, Λ_{ii}, are given by the following equation:

$$\Lambda_{ii}=\frac{RT}{f_i^m\upsilon_i}\frac{N_i^e}{N_i}\phi_i \qquad i=\text{s,f} \tag{10}$$

Here, f_i^m is the monomeric friction coefficient of component i as if it were a Rouse chain, N_i^e is the number of repeat units between entanglements for component i, and ϕ_i and υ_i are the molar fraction and molar volume of polymer i, respectively. If the polymer pair is completely miscible, such as PS/PVME or PVC/PMMA, then only one monomeric friction coefficient is sufficient to describe the diffusion process assuming that the polymer pair is homogeneous on a molecular scale. This assumption is in accordance with the reptation theory in which the motion of a chain is constrained within a tube defined by the chains in the surrounding matrix. In other words, reptation assumes that the diffusion of a chain is

strongly coupled with the properties of the matrix surrounding the chain. The implications of this assumption are that the diffusion of a chain is dominated by the chain molecular weight, the mesh size of the entangled chains and the compositon of the matrix, and is relatively independent of the monomer structure of the diffusing chain.

Roland and Ngai[32] measured the segmental relaxation in PS/PVME blend using dielectric spectroscopy. According to their results there was significant coupling and intersegmental cooperativity in the relaxation spectrum of this blend. This clearly indicates that the mobility of a chain in the PS/PVME matrix is strongly influenced by the other component and suggests that the friction coefficients f_s and f_f should be identical but a strong function of the matrix composition. Therefore, for completely miscible polymer pairs, equation (10) reduces to the following:

$$\Lambda_{ii}=\frac{RT}{f_b^m \upsilon}\frac{N_b^e}{N_i}\phi_i \qquad i=s,f \tag{11}$$

Here, f_b^m is the molar monomeric friction coefficient for the blend, which is strongly composition-dependent for a polymer pair with dissimilar physical properties. The parameter N_b^e is the average number of repeat units between entanglements for the blend, which is also a function of composition.

Composto and associates[33-35] investigated interdiffusion in a polymer pair consisting of PS as the slower-diffusing component with a T_g of 105°C and poly(xylenyl ether) (PXE) as the faster-diffusing component with a T_g of 216°C. Their results show that the concentration profile for this polymer pair is also asymmetric with swelling of the slower-diffusing component, PXE, by the faster-diffusing component, PS[33]. The same group[34] measured the tracer diffusion coefficient of PS and PXE by contacting a film containing blends of PS/PXE of varying composition with a deuterated PS or PXE (d-PS or d-PXE) film. They claimed that when a d-PS or d-PXE film was in contact with a PS/PXE film, they could measure the tracer diffusion coefficient of the d-PS or d-PXE chains, respectively. They reported that the monomeric friction coefficient of PS and PXE chains differed by as much as three orders of magnitude depending on composition. However, it is not clear how they can deduce the tracer diffusion coefficient of each polymer from their experiments because in polymer pairs with dissimilar properties the faster-diffusing component dominates the diffusion process at these interfaces. Moreover, they used the Fickian model to analyse their experimental results, which is not applicable to these interfaces. It was shown in a previous paper by us[11] that interdiffusion in dissimilar polymer pairs, such as PS/PVME, can have as much as 70% non-Fickian component, making the Fickian model inapplicable to these interfaces. They proposed[34] that the large difference in monomeric friction coefficients of the two polymers is caused by internal barriers to bond rotation, indicating that the temperature dependence of the friction coefficients should be different for each polymer. However, they observed experimentally that the temperature dependences of the friction coefficients were identical. In a subsequent work[35], they also used a combination of reptation and constrained release models to predict the molecular-weight and concentration dependence of interdiffusion at PS/PXE interfaces. However, the model was not successful because an unusually large number of constraints had to be used to predict the tracer diffusion coefficient of each polymer.

The model we present here is based on the assumption that the tracer diffusion coefficient of the two polymers is strongly coupled to the properties of the matrix. Thus, the chain diffusion coefficient is related to the chain molecular weight, the mesh size of the entangled chains and the composition of the matrix, and is relatively independent of the monomer structure of the diffusing chain.

Flux of each component

Substituting the fluxes from equation (6), the chemical potential gradients from equation (7) and the Onsager coefficients from equation (11) into equation (8) results in a relation between the total flux of the slower-diffusing component and the molecular parameters of each polymer:

$$j_s^L=-\left(\frac{RTN_b^e}{\upsilon f_b^m}\right)\left(\frac{1-\phi_s}{N_s}+\frac{\phi_s}{N_f}\right)\times\left(\frac{1-\phi_s}{N_s}+\frac{\phi_s}{N_f}+2\chi_{sf}\phi_s(1-\phi_s)\right)\Delta\phi_s \tag{12}$$

The time and spatial dependence of the mole fraction of the slow component can be obtained by substituting for the total flux from equation (12) into equation (9):

$$\frac{\partial\phi_s}{\partial t}=\frac{\partial}{\partial z}\left[\left(\frac{RTN_b^e}{f_b^m}\right)\left(\frac{1-\phi_s}{N_s}+\frac{\phi_s}{N_f}\right)\times\left(\frac{1-\phi_s}{N_s}+\frac{\phi_s}{N_f}+2\chi_{sf}\phi_s(1-\phi_s)\right)\Delta\phi_s\right] \tag{13}$$

The above equation relates the time and spatial dependence of the slower-diffusing component to molecular properties such as molecular weight, compatibility parameter, temperature and the blend friction coefficient. The first term accounts for the mobility of the polymer chains via the monomeric friction coefficient f_b^m; the second term accounts for the differences in molecular weight of the two polymers; and the third term accounts for the free energy of mixing. If the two polymers have similar physical properties but different molecular weights, then the second term is the dominant term, as in the case of the fast-mode theory[17,18]. However, if the two polymers have widely different physical properties, then the first term dominates.

Estimation of friction coefficients

Once a mechanism of motion is chosen for the polymer chains, the friction coefficient can be related to zero-shear viscosity. In turn, the zero-shear viscosity can be related to the volumetric properties of the blend, which are available in the literature for PS/PVME and PVC/PMMA blends. For the reptation model, the zero-shear viscosity is related to the friction coefficient by the following

equations[36]:

$$\eta_0^i = (\pi^2/15) k_B T v_i N_i^{seg} \tau_d^i \quad (14)$$

where

$$\tau_d^i = \frac{L_i^2 N_i}{\pi^2 k_B T} f_i^m \quad (15)$$

Here, η_0^i is the zero-shear viscosity of component i, which is composition-dependent, τ_d^i is the reptation time of chain i, N_i^{seg} is the number of statistical segments per chain, k_B is the Boltzmann constant and L_i is the contour length of polymer i. Equation (14) relates the zero-shear viscosity of a polymer to its reptation time and, in turn, equation (15) relates the reptation time of a chain to its monomeric friction coefficient. The chain contour length L_i and the number of statistical segments N_i^{seg} are related to the mesh size of the entangled chains a_i by the following equations:

$$L_i = \frac{5}{4}(N_i/N_i^e) a_i \quad (16)$$

$$N_i^{seg} = N_i b_i^2 / a_i^2 \quad (17)$$

Here, b_i is the statistical segment length. Rearranging equations (14) to (17) results in a relationship between the zero-shear viscosity and the monomeric friction coefficient:

$$f_i^m = \frac{48}{5} \frac{V_i^m (N_i^e)^2}{b_i^2 N_i^3} \eta_0^i \quad (18)$$

Here, V_i^m is the molar volume of component i. The above equation relates the molar monomeric friction coefficient of component i to its corresponding zero-shear viscosity.

This equation can be generalized to polymer blends that are completely miscible:

$$f_b^m = \frac{48}{5} \frac{V_b^m (N_b^e)^2}{b_b^2 N_b^3} \eta_0^b \quad (19)$$

Here, V_b^m is the molar average blend specific volume, N_b is the blend weight-average number of repeat units and η_0^b is the blend zero-shear viscosity. Generalization of equation (18) to miscible polymer blends simply states that polymer relaxation is dominated by the friction coefficient between the chains assuming there is no change in the mechanism of motion on blending. The molar volumes of the components of the PS/PVME[37] and PVC/PMMA[38] pairs are given in *Tables 1* and *2*, respectively. The number of repeat units between the entanglements for the blend can be estimated from the relationship between the entanglement molecular weight and the plateau modulus[39]:

$$\frac{1}{N_b^e} = \left(\frac{\phi_s}{(N_s^e)^{1/2}} + \frac{\phi_f}{(N_f^e)^{1/2}} \right)^2 \quad (20)$$

The number of repeat units between entanglements of each polymer for PS/PVME[40,41] and PVC/PMMA[41] pairs are presented in *Tables 1* and *2*, respectively. The statistical segment length for PS and PVME, measured by small-angle neutron scattering[42], is 7.8 Å, which is independent of composition. This value was also used for the PVC/PMMA pair as given in *Table 2*. Data are available in the literature for zero-shear viscosity of individual polymers such as PS[43] and PVME[40], but very limited data are available for zero-shear viscosity of polymer blends.

Table 1 Properties of PS and PVME at 125°C

Parameter	PS	PVME	Ref.
Molar volume, V_m ($cm^3\ mol^{-1}$)	104.1	60.4	37
Entanglement molecular weight, N_e ($g\ mol^{-1}$)	272	137	40,41
Statistical segment length, b (Å)	7.8	7.8	42
B_1 (eqn (21)) (dimensionless)	1.004	1.004	44
a (eqn (26)) (dimensionless)	3.42	3.50	40,45
K (eqn (26)) ($kg\ m^{-1}\ s^{-1}$)	1.10×10^{-13}	6.75×10^{-15}	40,45
C_1^i (eqn (25)) (dimensionless)	9.3	4.01	40,41
C_2^i (eqn (25)) (°C)	77.0	136.9	40,41
T_r (eqn (25)) (°C)	125.0	80.6	40,41

Table 2 Properties of PVC and PMMA at 120°C

Parameter	PVC	PMMA	Ref.
Molar volume, V_m ($cm^3\ mol^{-1}$)	46.0	86.9	38
Entanglement molecular weight, N_e ($g\ mol^{-1}$)	112	150	41
Statistical segment length, b (Å)	7.8	7.8	42
B_1 (eqn (21)) (dimensionless)	1.004	1.004	44
a (eqn (26)) (dimensionless)	3.4	3.4	41
K (eqn (26)) ($kg\ m^{-1}\ s^{-1}$)	9.02×10^{-11}	5.00×10^{-12}	41
C_1^i (eqn (25)) (dimensionless)	8.86	8.86	41
C_2^i (eqn (25)) (°C)	101.6	101.6	41
T_r (eqn (25)) (°C)	122.0	160.0	41

Estimation of blend zero-shear viscosity

The zero-shear viscosity for a blend can be related to its blend specific volume using the free-volume theory and the Doolittle equation:

$$\ln \eta_0^b = \frac{V_{o,b}}{V_{f,b}} B_1 + B_2 \quad (21)$$

Here, η_0^b, $V_{o,b}$ and $V_{f,b}$ are the blend zero-shear viscosity, blend occupied volume and blend free volume, respectively. The parameters B_1 and B_2 are constants in the Doolittle equation. The empirical constant B_1 is independent of the nature of the system and temperature and is equal to unity for most polymers[44], as given in *Tables 3* and *4* for PS/PVME and PVC/PMMA pairs, respectively. Assuming that the occupied volume and the empirical constant B_2 for the blend are additive quantities based on molar fraction, the zero-shear viscosity of the

Table 3 Composition dependence of the specific volume V_b, excess volume of mixing ΔV_b and expansion coefficient α for a PS/PVME pair at 125°C

PVME weight fraction	Specific volume, V_b ($cm^3\ g^{-1}$)	Excess volume of mixing, $\Delta V_b \times 10^3$ ($cm^3\ g^{-1}$)	Expansion coefficient, $\alpha \times 10^4$ (K^{-1})
0.00	1.0005	0.00	5.408
0.20	1.0022	−6.53	5.561
0.45	1.0144	−4.61	5.609
0.75	1.0303	−1.05	5.880
1.00	1.0416	0.00	6.245

Table 4 Composition dependence of the specific volume V_b excess volume of mixing ΔV_b and expansion coefficient α for a PVC/PMMA pair at 120°C

PVC weight fraction	Specific volume, V_b ($cm^3\ g^{-1}$)	Excess volume of mixing, $\Delta V_b \times 10^3$ ($cm^3\ g^{-1}$)	Expansion coefficient, $\alpha \times 10^4$ (K^{-1})
0.00	0.8686	0.00	6.73
0.20	0.8436	1.50	6.02
0.50	0.8005	−1.80	5.93
0.80	0.7580	−4.40	5.62
1.00	0.7359	0.00	5.35

blend is given by the following relation:

$$\ln \eta_0^b = \sum_{i=1}^{2} \phi_i \ln \eta_0^i + \frac{\sum_{i=1}^{2} \omega_i \gamma_i V_i}{V_b - \sum_{i=1}^{2} \omega_i \gamma_i V_i} - \frac{1}{2} \sum_{i=1}^{2} \phi_i (\delta_i - 1) \tag{22}$$

Here

$$\gamma_i = \frac{\delta_i - 1}{\delta_i + 1} \tag{23}$$

where

$$\delta_i^2 = 1 - \frac{4\, \partial \ln \eta_0^i / \partial T}{B_1\, \partial \ln V_i / \partial T} \tag{24}$$

The first term in equation (22) accounts for the differences in zero-shear viscositiy of each component, the second term accounts for the variation of blend specific volume with composition, and the third term accounts for the differences in thermal expansion coefficient of each component. The blend specific volume V_b is presented in *Tables 3* and *4* as a function of composition for the PS/PVME[40] and PVC/PMMA[38] pairs, respectively. The zero-shear viscosities of individual components were corrected for temperature and molecular weight by the Williams–Landel–Ferry (WLF) equation and a scaling law for well entangled polymer melts, respectively:

$$\log\left(\frac{\eta_{0,T}^i}{\eta_{0,T_r}^i}\right) = \frac{-C_1^i (T - T_r^i)}{C_2^i + (T - T_r^i)} \tag{25}$$

$$\eta_0^i = K_i M_i^{a_i} \tag{26}$$

Here, K_i and a_i are empirical constants for component i, C_1^i and C_2^i are empirical constants for the WLF equation for component i, and B_1 is the empirical constant for the Doolittle equation. These constants for PS/PVME[40,41] and PVC/PMMA[45] pairs are given in *Tables 1* and *2*, respectively.

Differential equation and boundary conditions

The partial differential equation describing the diffusion process at the interface between two compatible polymers is given by equation (13) and can be expressed in the following form after differentiation with respect to the z axis:

$$\frac{\partial \phi_s}{\partial t} = D \frac{\partial^2 \phi_s}{\partial z^2} + \frac{\partial D}{\partial \phi_s}\left(\frac{\partial \phi_s}{\partial z}\right)^2 \tag{27}$$

where

$$D = \left(\frac{RTN_b^e}{f_b^m}\right)\left(\frac{1-\phi_s}{N_s} + \frac{\phi_s}{N_f}\right)\left(\frac{1-\phi_s}{N_s} + \frac{\phi_s}{N_f} + 2\chi_{sf}\phi_s(1-\phi_s)\right) \tag{28}$$

The blend molar monomeric friction coefficient f_b^m is defined by equation (19). The initial and boundary conditions for solving the above diffusion equation are:

$$t = 0 \qquad \phi_f = 0 \qquad \text{for } 0 \leqslant z < \delta_s \tag{29}$$

$$t = 0 \qquad \phi_f = 1 \qquad \text{for } \delta_s \leqslant z \leqslant \delta_s + \delta_f \tag{30}$$

$$z = 0 \qquad \partial \phi_f / \partial z = 0 \qquad \text{for } t > 0 \tag{31}$$

$$z = \delta_s + \delta_f \qquad \partial \phi_f / \partial z = 0 \qquad \text{for } t > 0 \tag{32}$$

The boundary conditions (31) and (32) represent no-flux boundary conditions.

It is important to recognize the importance of each term on the right-hand side of equation (27). The first term represents interdiffusion at the interface between the two polymers while the second term represents the swelling of the slower-moving component by the faster-moving component. For homopolymers with different molecular weights or polymer pairs with similar properties, the two terms are of the same order of magnitude and the concentration profile is symmetric. However, for polymer pairs with dissimilar properties, such as PS and PVME, the second term dominates as the faster component swells the slower component and the diffusion equation becomes highly stiff.

The above differential equation is solved with a variable-step-size finite-difference method. For the PS/PVME pair with dissimilar properties the differential equation becomes stiff and the second initial condition, equation (30), is a measure of the stiffness for the differential equation. For example, for the PS/PVME pair at $t = 0$ and $\phi_f = 0.25$, the maximum variation in PVME mole fraction is 0.25 and the diffusion coefficient changes by two orders of magnitude across the interface at 125°C, and only 100 grid points are required. However, for the same polymer pair at $t = 0$ and $\phi_f = 1.0$, the maximum variation in PVME mole fraction is 1.0 and the diffusion coefficient changes by six orders of magnitude across the interface at 125°C, and 10 000 grid points are required. For the PS/PVME pair, where the

diffusion coefficient changes by six orders of magnitude at 125°C, the PVME mole fraction in the second boundary condition, equation (30), was increased from 0.25 to 1.0 in steps of 0.005 until convergence was achieved.

EXPERIMENTAL

Sample preparation

Polystyrene (PS) was obtained from Pressure Chemical Co. (Pittsburgh, PA) as a primary standard with number-average molecular weight $\overline{M}_n$ of 1.0×10^5 and polydispersity index *PI* of 1.06. The PVME was obtained from Scientific Polymer Products (Ontario, NY) as a secondary standard with $\overline{M}_n$ of 4.7×10^4 and *PI* of 2.10. Gel permeation chromatography was carried out in a chromatograph (model 6000A, Waters Associates, Milford, MA) using tetrahydrofuran as the mobile phase and μStyragel® columns with 10^6, 10^5, 10^4, 10^3 Å pore sizes and 1 ml min^{-1} flow rate. It indicated that no additives were present in the polymer. The PS and PVME samples had T_g of 101°C and −27°C, respectively, measured by differential scanning calorimetry (DSC 2910, TA Instruments, Wilmington, DE). A thermogravimetric analyzer (Hi-Res TGA 2950, TA Instruments, Wilmington, DE) was used to study the degradation behaviour of PVME and its blends with PS as a function of temperature. According to t.g.a. results, the PVME is stable for at least 4 h at 105°C, with increased stability at lower temperatures.

An *FT*i.r. spectrometer (Nicolet 800, Madison, WI) with the a.t.r. accessory (Connecticut Instruments, Boston, MA) were used for the interdiffusion studies in the configuration shown in *Figure 2*. The a.t.r. crystal was germanium (Ge) with 5 cm length, 1 cm width and 2 mm thickness. A PS film was cast from a 5 wt% *p*-xylene solution on an a.t.r. crystal with a spin coater (model 1-EC101D-R485, Photo-Resist Spinners, Garland, TX) from *p*-xylene solution at 250 rev min^{-1}. The PS film was dried in a controlled atmosphere at 25°C for at least 24 h, then *in vacuo* at 25°C for 24 h, followed by *in vacuo* at 115°C for 1 h to remove any residual solvent in the film. The film was then annealed at 115°C for at least 12 h to remove solvent and to minimize molecular orientation resulting from the spinning process. The thickness of the PS film was 0.7 μm measured with a profilometer (Alpha-Step 200, Tencor Instruments, Mountain View, CA).

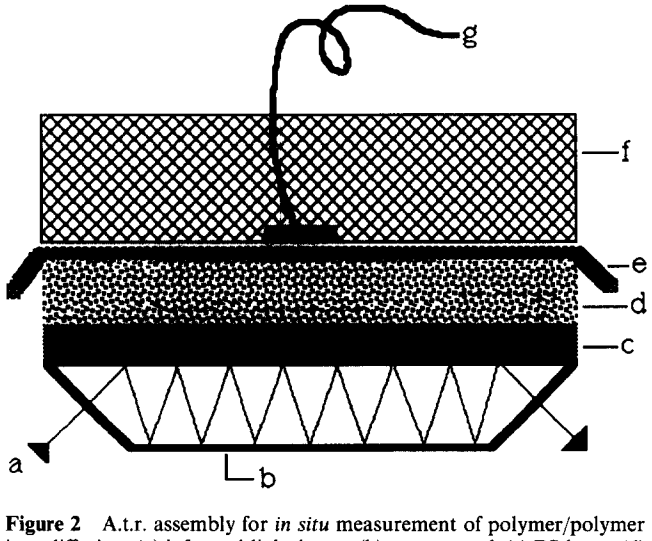

Figure 2 A.t.r. assembly for *in situ* measurement of polymer/polymer interdiffusion: (a) infra-red light beam; (b) a.t.r. crystal; (c) PS layer; (d) PVME layer; (e) aluminium foil; (f) heating unit; (g) thermocouple

The PVME was cast directly on the PS film from a 10 wt% isobutanol solution using a spin coater at 250 rev min^{-1}. The PVME film was dried at 25°C for 24 h and then *in vacuo* at room temperature for 24 h to remove residual water. Since the T_g of PVME is below room temperature, further drying at higher temperatures was not necessary. The thickness of the PVME film was measured by casting a PVME film on a microscope slide, with the same dimensions as the a.t.r. crystal and under the same spinning conditions. The film was dried at 25°C for 24 h and then *in vacuo* at room temperature for 24 h to remove residual water. The glass slide was weighed before and after the PVME film was cast. The thickness of the PVME film was 6.6 μm, determined from the weight of PVME and the dimensions of the glass slide.

Attenuated total reflection infra-red spectroscopy

The use of a.t.r.-*FT*i.r. for interdiffusion studies at polymer/polymer interfaces has been described by us before[11]. Briefly, the infra-red beam enters the a.t.r. crystal from one of the side faces. If the refractive index of the crystal is higher than that of PS and the incident angle of the beam is higher than the critical angle, then the infra-red beam is totally reflected at the crystal/PS interface and the beam travels inside the crystal and exits from the other side face. However, at the crystal/polymer interface, a small fraction of the beam penetrates into the PS layer and is absorbed by PS. The fraction of the beam that is absorbed gives rise to absorption bands in the a.t.r. spectrum and is used to monitor the concentration of each component within the penetration depth in the polymer layer.

In a typical experiment, a PS film was cast by spin coating from *p*-xylene solutions on a Ge crystal. The PS film was dried in a controlled atmosphere to remove any residual solvent. The PVME was spin cast directly on the PS film from isobutanol solution to ensure good adhesion and molecular contact at the PS/PVME interface. The assembly consisting of the a.t.r. crystal, the two polymer films, the aluminium foil and the heating unit was heated to the desired interdiffusion temperature and the a.t.r.–*FT*i.r. spectrum was collected *in situ* with 128 averaged scans and a resolution of 4 cm^{-1}. The end-face angle of the a.t.r. crystal and the optical angle of the infra-red beam were 45°.

ANALYSIS OF EXPERIMENTAL RESULTS

Spectral analysis

The a.t.r.-*FT*i.r. spectra of PS and PVME in the high-frequency region and the assignment of each absorption band have been discussed elsewhere[11]. The a.t.r.-*FT*i.r. spectrum of a 50/50 w/w PS/PVME blend in the high-frequency region from 2700 to 3200 cm^{-1} is shown in *Figure 3*. The PVME band at 2820 cm^{-1} and the PS bands at 2850 and 3030 cm^{-1} were used for quantitative analysis of the PS/PVME spectra.

Time evolution of the a.t.r.-*FT*i.r. spectrum for interdiffusion in the PS/PVME pair at 105°C is shown

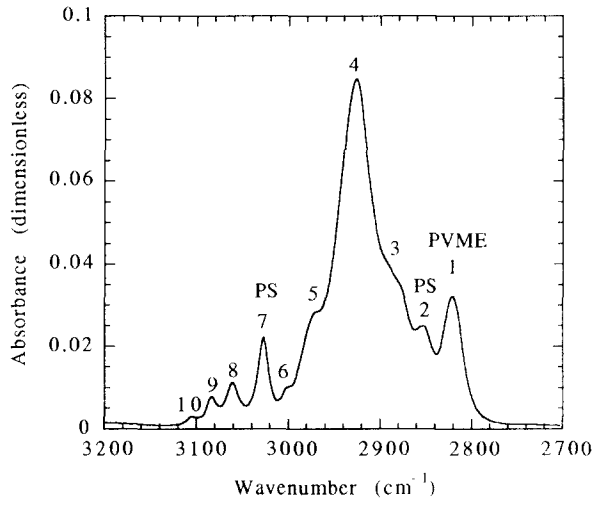

Figure 3 A.t.r.-*FT*i.r. spectrum of a 50/50 w/w PS/PVME mixture in the high-frequency region. The peak frequencies 1 to 10 are 2820, 2850, 2880, 2930, 2975, 3000, 3030, 3060, 3085 and 3105 cm^{-1}, respectively

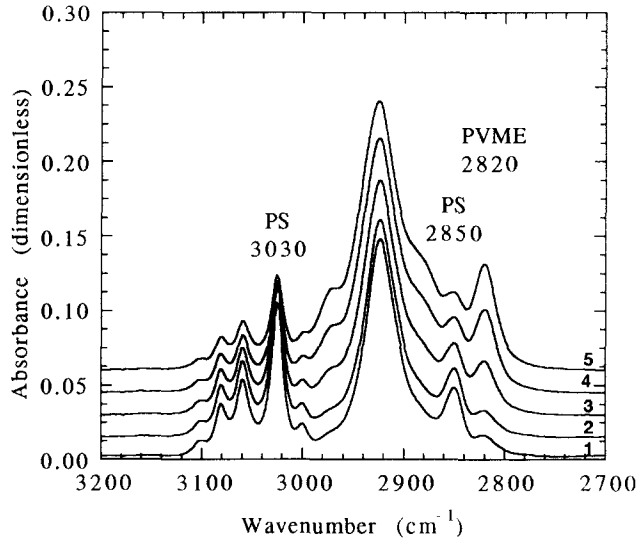

Figure 4 Time evolution of a.t.r.-*FT*i.r. spectra for interdiffusion in a PS/PVME pair at 105°C. The PS and PVME molecular weights $\overline{M}_w$ were 1.05×10^5 and 9.9×10^4 with polydispersity indices of 1.06 and 2.10, respectively. The PS film was spin cast on a Ge crystal at 250 rev min^{-1} from a 5 wt% *p*-xylene solution. The PVME film was spin cast on the PS film at 250 rev min^{-1} from a 10% isobutanol solution. The PS and PVME film thicknesses were 0.7 μm and 6.6 μm, respectively. The absorbance scale corresponds to spectrum 1 and the other spectra are shifted by 0.015 absorbance units. The spectra 1 to 5 correspond to 0, 14, 28, 42 and 56 min of interdiffusion time, respectively

in *Figure 4*. The absorbance scale corresponds to the spectrum at zero interdiffusion time. The other spectra were shifted by 0.015 absorbance units for visual clarity. The spectra 1 to 5 correspond to 0, 14, 28, 42 and 56 min of interdiffusion time, respectively. For quantitative analysis, the PS/PVME spectrum was deconvoluted to relate the area under the three peaks to PS and PVME mole fractions. The deconvolution program uses the Levenberg–Marquardt fitting routine to fit the experimental convoluted absorbance data to a set of calculated Gaussian or Lorentzian peaks[11]. The best fit was obtained with a 50% Lorentzian and 50% Gaussian peak composition.

To relate the molar fraction of PVME to the relative absorbance of PVME and PS, a calibration curve was required. Blends of PS and PVME with known composition ranging from 10% to 90% PS by weight were cast on a ZnSe crystal from a 1% solution in toluene at 250 rev min^{-1}. Toluene is a compatible solvent for PS as well as PVME. The areas under the peaks were determined by deconvoluting the original spectrum. The areas of the PVME band at 2820 cm^{-1} and of the PS bands at 2850 and 3030 cm^{-1} were used to calculate the relative absorption of PVME and PS.

*A.t.r.-*FT*i.r. cumulative concentration*

The relative intensity of i.r. radiation decreases exponentially as a function of distance away from the crystal surface and is characterized by the penetration depth of the radiation within the polymer film. This exponential decrease has to be considered in order to compare experimental results with the model predictions. For an interdiffusion time t, the mole fraction of PVME from the model, ϕ_f, at distance z was multiplied by its corresponding relative intensity and it was integrated over the penetration depth. This process was repeated for each interdiffusion time to give the cumulative concentration of PVME, Q_f, *versus* time as given by the following equation:

$$Q_f(t) = \frac{\int_0^\infty \phi_f(z,t) I_{rel}(z)\, dz}{\int_0^\infty I_{rel}(z)\, dz} \tag{33}$$

where

$$I_{rel} = \exp(-z/d_p) \tag{34}$$

Here, I_{rel} is the i.r. intensity relative to the intensity at the interface, z is the distance from the crystal/polymer interface in the polymer layer, and d_p is the penetration depth of i.r. radiation in the polymer medium. The penetration depth d_p for Ge crystal with end-face and optical angle of 45° is 0.11 μm for the PS/PVME pair and 3000 cm^{-1} i.r. frequency.

RESULTS AND DISCUSSION

Concentration profile for PS/PVME interface

The properties of PS and PVME for simulating interdiffusion at the PS/PVME interface at 125°C are given in *Table 1*. The PS and PVME were monodisperse with molecular weights $\overline{M}_w$ of 1.05×10^5 and 9.9×10^4, respectively. The molecular weights for entanglement of PS and PVME were 17 500 and 4600, respectively. The Flory–Huggins interaction parameter and the lower critical solution temperature (*LCST*) for this pair are independent of molecular weight[46] for PS and PVME molecular weights above 5.0×10^4. The temperature dependence of the Flory–Huggins interaction parameter for the PS/PVME pair is given by the following relation[47]:

$$\chi/v_{0,b} = 10.6 \times 10^{-4} - 0.436/T \tag{35}$$

Here, $v_{0,b}$ is the blend specific molar volume. The specific volume V_b, the excess volume of mixing ΔV_b and the expansion coefficient α for the PS/PVME pair as a function of composition for predicting the composition

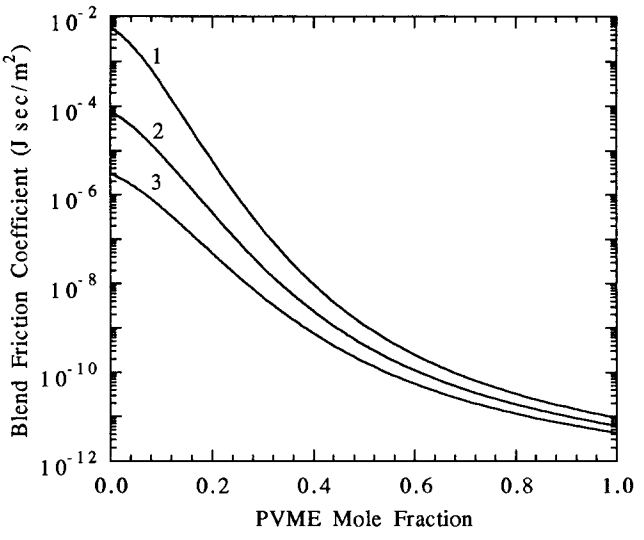

Figure 5 Composition dependence of the monomeric friction coefficient for the PS/PVME pair at 105°C (curve 1), 115°C (curve 2) and 125°C (curve 3). For the simulation, PS and PVME were monodisperse with molecular weights $\overline{M_w}$ of 1.05×10^5 and 9.9×10^4, respectively

dependence of the zero-shear viscosity are shown in *Table 3*. The excess volume of mixing for this pair is negative at 125°C. The temperature dependence of the specific volume as a function of composition was evaluated using the blend specific volume and the expansion coefficient.

The variation of the monomeric friction coefficients with composition, predicted using equation (19), is shown in *Figure 5*. The blend monomeric friction coefficient changes by six, seven and eight orders of magnitude at 125°C, 115°C and 105°C, respectively. As PVME is added to a PS matrix, the friction coefficient decreases dramatically owing to the high mobility and low T_g of PVME and the friction coefficient becomes dominated by the physical properties of PVME. For example, increasing the PVME mole fraction from 0 to 0.4 at 125°C reduces the friction coefficient by four orders of magnitude, whereas increasing the PVME mole fraction from 0.4 to 1.0 reduces the friction coefficient only by one order of magnitude. This clearly indicates that PVME plasticizes the PS matrix as interdiffusion takes place across the interface. Therefore, for polymers with dissimilar physical properties, interdiffusion is accompanied by swelling of the slower-diffusing component, here PS, by the faster-diffusing component, here PVME.

Green *et al.*[48] measured the tracer diffusion coefficient of PS in PS/PVME matrices of different composition with forward recoil spectrometry and they evaluated the monomeric friction coefficient for PS as a function of matrix composition using the reptation theory. The predicted PS monomeric friction coefficient is compared with the experimental data of Green *et al.* in *Figure 6* for the PS/PVME pair at 125°C. The predicted and the experimental friction coefficients are qualitatively in good agreement and the model can successfully predict the composition dependence of the monomeric friction coefficient. The model deviates from the experimental values by one order of magnitude, especially at high PVME concentrations. This deviation can be attributed to the PVME sample for the experimental data of Green *et al.*, which had a polydispersity index of 2.10.

To illustrate the asymmetry of the concentration profile predicted by the model, *Figure 7* compares the simulated PVME concentration profile at 125°C after 1 s with the Fickian model prediction with constant diffusion coefficient of 1.0×10^{-13} cm^2 s^{-1}. The distance from the interface was normalized based on the film thickness of the slower-diffusing polymer, PS. The dimensionless time t^* was defined based on the following equation:

$$t^* = tD_{PVME}/\delta_s^2 \tag{36}$$

Here, D_{PVME} is the self-diffusion coefficient of PVME. According to this figure, the concentration profile for the

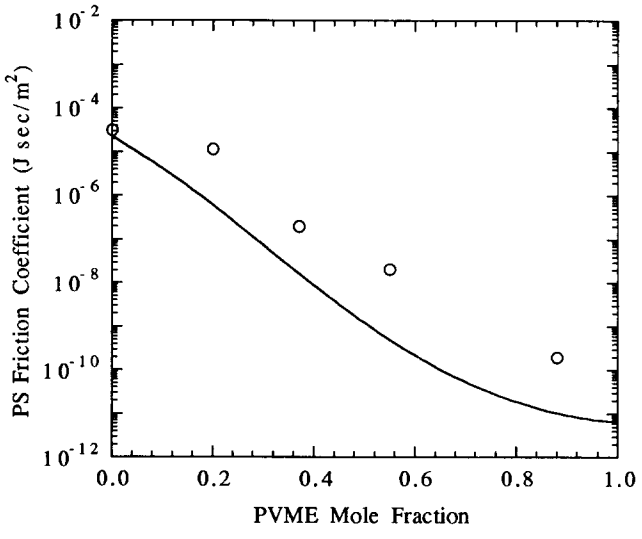

Figure 6 Comparison of the predicted (full curve) and experimental (open circles) monomeric friction coefficient for the PS/PVME pair at 120°C. The predicted values were based on equation (19). For the simulation, PS and PVME were monodisperse with molecular weights $\overline{M_w}$ of 1.05×10^5 and 9.9×10^4, respectively. The experimental data points were extracted from Green *et al.*[48] with PS and PVME $\overline{M_w}$ of 1.05×10^5 and 9.9×10^4 and polydispersity indices of 1.06 and 2.10, respectively

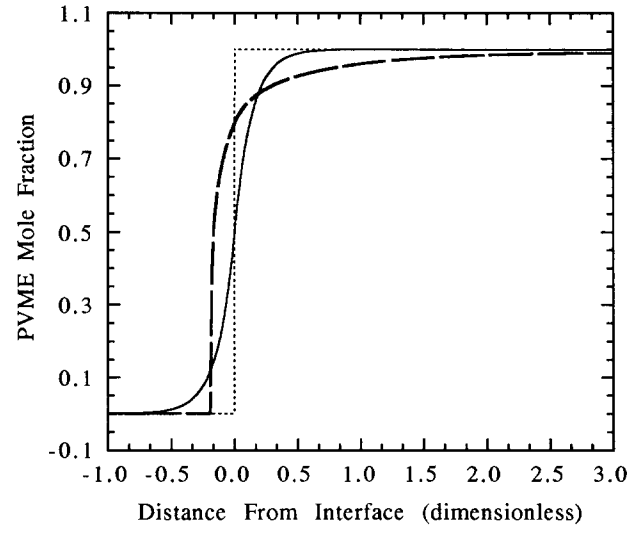

Figure 7 Comparison of the simulated (thick broken curve) concentration profile and the Fickian model with constant diffusion coefficient of 1.0×10^{-13} cm^2 s^{-1} (thin full curve) for the PS/PVME pair at 125°C. The dotted curve is the original interface. For the simulation, PS and PVME were monodisperse with molecular weights $\overline{M_w}$ of 1.05×10^5 and 9.9×10^4, respectively. The distance from the interface was normalized based on the PS film thickness

Fickian model with constant diffusion coefficient (thin full curve) is symmetric whereas the simulated profile (thick broken curve) is asymmetric, with the original interface moving into the slower-diffusing polymer as a swelling front. Time evolution of the simulated PVME concentration profile at 125°C is shown in *Figure 8* for dimensionless times of 0.05, 0.50, 1.50 and 6.0. This figure shows that the concentration profile remains unsymmetric as interdiffusion proceeds and the interface moves like a swelling front into the PS layer.

The experimental time evolution of PVME concentration for the PS/PVME pair at 105°C after analysis of the spectra in *Figure 4* is shown in *Figure 9*. This figure compares the simulated cumulative concentration of PVME (full curve) at 125°C with experimental results from a.t.r.-*FT*i.r. (open circles) at 105°C. The dotted curve is the Fickian model prediction with constant diffusion coefficient. The simulated and experimental data were normalized for time and temperature using equation (36). If the interface moves as a sharp front into the PS layer, such as the simulated PS/PVME interface shown in *Figure 8*, the PVME cumulative concentration is characterized by an induction time for the interface to reach the penetration depth of i.r. radiation and then the PVME concentration increases sharply. On the other side, if the interface is diffuse as interdiffusion proceeds, such as in the Fickian model with constant diffusion coefficient, the cumulative concentration increases gradually with time. The experimental PVME cumulative concentration shows very good agreement with the simulated cumulative concentration shown in *Figure 8*, indicating that the interface moves as a sharp front into PS as predicted by the model. We believe that the discrepancy between the simulated and experimental cumulative concentration was due to polydispersity of PVME, which was 1.0 and 2.10 for the simulation and the experiment, respectively. Monodisperse PVME was not available to us to prove that the discrepancy between the simulated and experimental result was due to polydispersity, and a simulation with a polydisperse PVME required the numerical solution of multiple partial differential equations simultaneously, which was not feasible computationally.

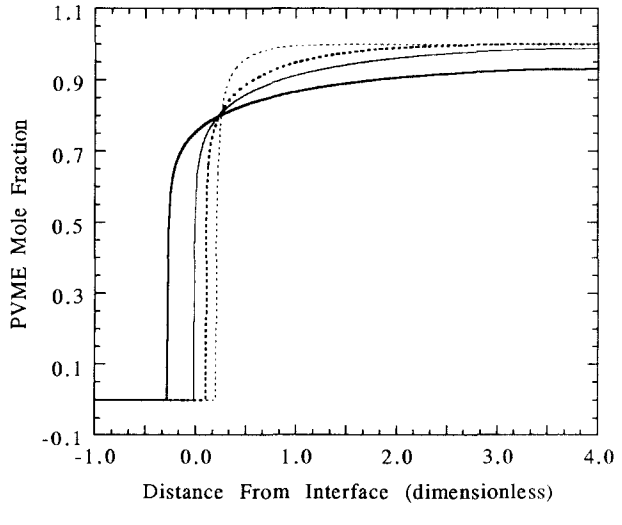

Figure 8 Time evolution of the concentration profile for the PS/PVME pair at 125°C. The thin dotted to thick full curves correspond to dimensionless times of 0.05, 0.5, 1.5 and 6.0, respectively. For the simulation, PS and PVME were monodisperse with molecular weights $\overline{M}_w$ of 1.05×10^5 and 9.9×10^4, respectively. The distance from the interface was normalized based on the PS film thickness. The dimensionless time t^* is defined by equation (36)

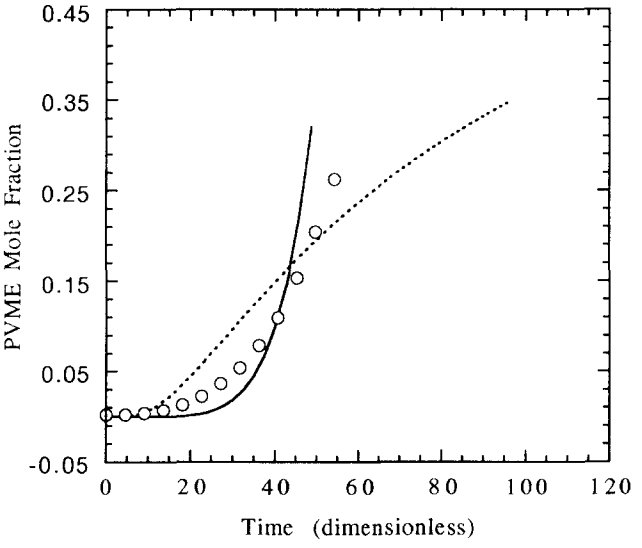

Figure 9 Comparison of the simulated cumulative concentration of PVME (full curve) with experimental PVME cumulative concentration (open circles) from a.t.r.-*FT*i.r. The dotted curve is the Fickian model prediction with constant diffusion coefficient of 1.0×10^{-13} cm^2 s^{-1}. For the simulation, PS and PVME were monodisperse with molecular weights $\overline{M}_w$ of 1.05×10^5 and 9.9×10^4, respectively. For the a.t.r.-*FT*i.r. experiment, the PS and PVME molecular weights $\overline{M}_w$ were 1.05×10^5 and 9.9×10^4 with polydispersity indices of 1.06 and 2.10, respectively. The PS film was spin cast on a Ge crystal at 250 rev min^{-1} from a 5 wt% *p*-xylene solution. The PVME film was spin cast on the PS film at 250 rev min^{-1} from a 10% isobutanol solution. The PS and PVME film thicknesses were 0.7 μm and 6.6 μm, respectively. The simulated and experimental data were normalized for time and temperature using equation (36)

Concentration profile for PVC/PMMA interface

The properties of PVC and PMMA for simulating interdiffusion at the PVC/PMMA interface at 120°C are given in *Table 2*. The PVC and PMMA were monodisperse with molecular weights $\overline{M}_w$ of 1.2×10^5 and 1.0×10^5, respectively. The molecular weights for entanglement for PVC and PMMA were 3100 and 15 000, respectively. The Flory–Huggins interaction parameter for this blend is reported by Shen *et al.*[49] to be twice the value for the PS/PVME blend. Therefore, the value of $\chi = 6.8 \times 10^{-3}$ was used for the simulation at 120°C. The specific volume, excess volume of mixing and the expansion coefficient for this pair as a function of composition for predicting the composition dependence of the zero-shear viscosity are shown in *Table 4*. The excess volume of mixing is slightly positive at lower PVC weight fraction, but it becomes negative at higher PVC fractions, which has a significant effect on the monomeric friction coefficient.

The composition dependence of the blend monomeric friction coefficient for the PVC/PMMA pair at 120°C is shown in *Figure 10*. The blend friction coefficient changes by two orders of magnitude at 120°C. This variation is smaller than for the PS/PVME pair owing to the similar physical properties of PVC and PMMA. The increase in blend friction coefficient for PVC mole fractions between

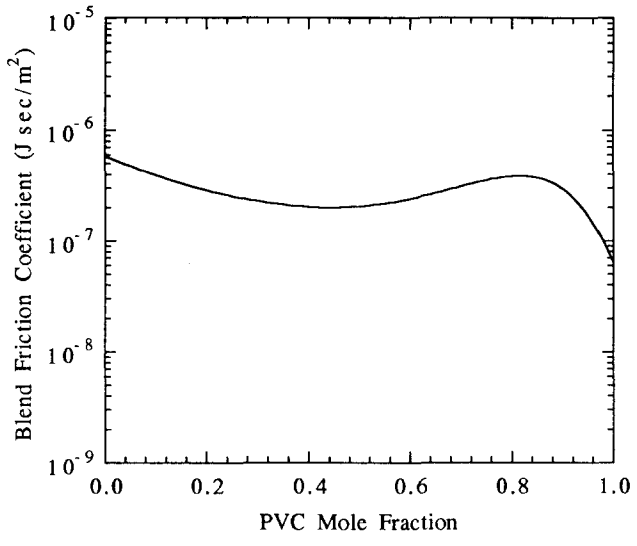

Figure 10 Composition dependence of the monomeric friction coefficient for the PVC/PMMA pair at 120°C. For the simulation, PVC and PMMA were monodisperse with molecular weights $\overline{M_w}$ of 1.2×10^5 and 1.0×10^5, respectively

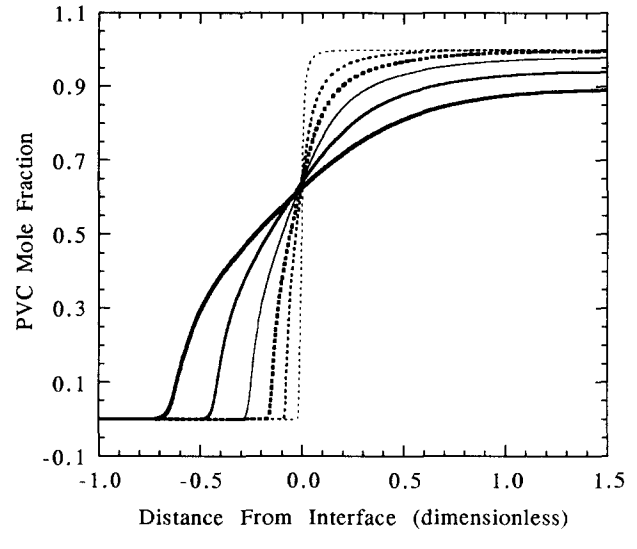

Figure 11 Time evolution of the concentration profile for the PVC/PMMA pair at 120°C. The thin dotted to thick full curves correspond to dimensionless times of 0.002, 0.006, 0.015, 0.04, 0.1 and 4.5, respectively. For the simulation, PVC and PMMA were monodisperse with molecular weights $\overline{M_w}$ of 1.05×10^5 and 9.9×10^4, respectively. The distance from the interface was normalized based on the PS film thickness. The dimensionless time t^* is defined by equation (36)

0.7 and 0.9 is due to the negative volume of mixing in this concentration range (see *Table 2*), which indicates that the change in volume of mixing on blending has a significant effect on the mobility of the chains. Time evolution of the simulated PVC concentration profile at 120°C is shown in *Figure 11* for dimensionless times of 0.002, 0.006, 0.015, 0.04, 0.1 and 4.5, which differ significantly from the profiles for the PS/PVME pair. This figure shows that the interface is more symmetric and diffuse compared with the PS/PVME pair owing to the similar properties of the PVC/PMMA pair. Comparison of the PVC/PMMA concentration profile with the PS/PVME profile clearly illustrates the effect of differences in physical properties of the two polymers on the shape and symmetry of these profiles.

CONCLUSIONS

The model was applied to the polymer pair PS/PVME with very dissimilar physical properties and to the polymer pair PVC/PMMA with similar properties, to predict the concentration profile at these interfaces. For the PS/PVME interface at 125°C, the blend monomeric friction coefficient changed by six orders of magnitude with composition. This indicated that, for interfaces between polymers with very dissimilar properties, the friction coefficients are highly composition-dependent. Also for the PS/PVME pair, the concentration profiles were asymmetric, with substantial swelling of the slower-diffusing component by the faster-diffusing component, and the original interface moved into the slower-diffusing phase as as swelling front. For the PVC/PMMA interface at 120°C, the blend monomeric friction coefficient varied by two orders of magnitude with composition, and the concentration profiles were symmetric compared with the PS/PVME pair.

REFERENCES

1 Binder, K. and Sillescu, H. in 'Encyclopedia of Polymer Science and Engineering', Wiley, New York, 1989, Vol. 20, p. 297
2 Kausch, H. H. and Tirrell, M. *Annu. Rev. Mater. Sci.* 1989, **19**, 341
3 Gilmore, P. T., Falabella, R. and Laurence, R. L. *Macromolecules* 1980, **13**, 880
4 Fytas, G. *Macromolecules* 1987, **20**, 1430
5 Voyutskii, S. S. *J. Adhesion* 1971, **3**, 69
6 Kim, J. K. and Han, C. D. *Polym. Eng. Sci.* 1991, **31**, 258
7 Green, P. F. and Doyle, B. L. *Macromolecules* 1987, **20**, 2471
8 Brochard-Wyart, F., Proc. Toyota Conf. *Stud. Polym. Sci.* 1988, **2**, 249
9 Brochard-Wyart, F. and de Gennes, P. G. *Makromol. Chem., Macromol. Symp.* 1990, **40**, 167
10 Brochard-Wyart, A. and Pincus, P. *C. R. Acad. Sci., Ser. II* 1992, **314**, 131
11 Jabbari, E. and Peppas, N. A. *Macromolecules* 1993, **26**, 2175
12 de Gennes, P. G. *C. R. Acad. Sci., Ser. II* 1981, **292**, 1505
13 Brochard-Wyart, F., Jouffroy, J. and Levinson, P. *Macromolecules* 1983, **16**, 1638
14 de Gennes, P. G. *J. Chem. Phys.* 1980, **72**, 4756
15 Tead, S.F. and Kramer, E. J. *Macromolecules* 1988, **21**, 1513
16 Green, P. F., Palmstrom, C. J., Mayer, J. W. and Kramer, E. J. *Macromolecules* 1985, **18**, 501
17 Kramer, E. J., Green, P. F. and Palmstrom, C. J. *Polymer* 1984, **25**, 473
18 Sillescu, H. *Makromol. Chem., Rapid Commun.* 1987, **8**, 393
19 Akcasu, A. Z., Nagele, G. and Klein, R. *Macromolecules* 1990, **24**, 4408
20 Seggern, J. V., Klotz, S. and Cantow, H. J. *Macromolecules* 1989, **22**, 3328
21 Jordan, E. A., Ball, R. C., Donald, A. M., Fettes, L. J., Jones, R. A. L. and Klein, J. *Macromolecules* 1988, **21**, 235
22 Reiter, G., Huttenbach, S., Foster, M. and Stamm, M. *Macromolecules* 1991, **24**, 1179
23 Foley, G. and Cohen, C. *J. Polym. Sci., Polym. Phys. Edn.* 1987, **25**, 2027
24 Sauer, B. B. and Walsh, D. J. *Macromolecules* 1991, **24**, 5948
25 Onsager, L. *Ann. NY Acad. Sci.* 1933, **34**, 241
26 Onsager, L. *Phys. Rev.* 1931, **37**, 405
27 Woolf, L. A., Miller, D. G. and Gosting, L. J. *J. Am. Chem. Soc.* 1962, **84**, 317
28 Cussler, E. L. 'Multicomponent Diffusion', Elsevier, Amsterdam, 1976, p. 1
29 Silberberg, A. *Polym. Prepr.* 1991, **32**(1), 495
30 Jabbari, E. and Peppas, N. A. *J. Mater. Sci.* 1994, **29**, 3969
31 Flory, P. J. 'Principles of Polymer Chemistry', Cornell University Press, Ithaca, NY, 1953, p. 495
32 Roland, C. M. and Ngai, K. L. *Macromolecules* 1992, **25**, 363
33 Composto, R. J. and Kramer, E. J. *J. Mater. Sci.* 1991, **26**, 2815

34 Composto, R. J., Kramer, E. J. and White, D. M. *Polymer* 1990, **331**, 2320
35 Composto, R. J., Kramer, E. J. and White, D. M. *Macromolecules* 1992, **25**, 4167
36 Graessley, W. W. *J. Polym. Sci., Polym. Phys. Edn.* 1980, **18**, 27
37 Tsujita, Y., Kato, M., Kinoshita, T. and Takizawa, A. *Polymer* 1992, **33**, 773
38 Sato, T., Tsujita, Y., Takizawa, A. and Kinoshita, T. *Macromolecules* 1991, **24**, 158
39 Creton, C., Kramer, E. J., Hul, C. Y. and Brown, H. R. *Macromolecules* 1992, **25**, 3075
40 Takahashi, Y., Suzuki, H., Naakagawa, Y., Yamaguchi, M. and Noda, I. *Polym. J.* 1991, **23**, 1333
41 Van Krevelen, D. W. 'Properties of Polymers', 3rd Edn., Elsevier, New York, 1990, p. 462
42 Shibayama, M., Yang, H., Stein, R. S. and Han, C. C. *Macromolecules* 1985, **18**, 2179
43 Watanabe, H., Yamazaki, M., Yoshida, H. and Kotaka, T. *Macromolecules* 1991, **24**, 5573
44 Aklonis, J. J. and MacKnight, W. J. 'Introduction to Polymer Viscoelasticity', 2nd Edn., Wiley, New York, 1983, p. 63
45 Potter, D. K. and Rudin, A. *Macromolecules* 1991, **24**, 213
46 Gelles, R. and Frank, C. W. *Macromolecules* 1983, **16**, 1448
47 Hammouda, B., Briber, R. M. and Bauer, B. J. *Polym. Commun.* 1994, **35**, 168
48 Green, P. F., Adolf, D. B. and Gilliom, L. R. *Macromolecules* 1991, **24**, 3377
49 Shen, S. and Torkelson, M. *Macromolecules* 1992, **25**, 721